Development 110, 115–130 (1990)
Printed in Great Britain © The Company of Biologists Limited 1990

The mechanics of notochord elongation, straightening and stiffening in the embryo of *Xenopus laevis*

DANY SPENCER ADAMS*, RAY KELLER† and M. A. R. KOEHL‡

Department of Zoology, University of California, Berkeley, CA 94720, USA

* Present address: Department of Zoology NJ-15, University of Washington, Seattle, WA 98250, USA
† Present address: Division of Cell and Developmental Biology, Department of Molecular and Cell Biology, University of California, Berkeley, CA 94720, USA
‡ Present address: Department of Integrative Biology, University of California, Berkeley, CA 94720, USA

Summary

We have examined the biomechanical development of the notochord of *Xenopus* early tail-bud embryos by: (1) quantifying morphological and mechanical changes in the embryo during stages 20–28, and (2) conducting manipulative experiments to elucidate mechanical roles of various components of the notochord. The notochord, which is composed of a stack of flat cells surrounded by a connective tissue sheath, elongates dramatically and begins straightening between stages 21 and 25. At this time the fiber density in the notochord sheath goes up, the osmotic activity of the notochord cells increases, vacuoles within these cells swell, the internal pressure of the notochord increases 2- to 3-fold, and the flexural stiffness of the notochord rises by an order of magnitude. We suggest that the tendency of the notochord cells to osmotically swell is resisted by the sheath, thereby permitting the internal pressure to rise. This pressure increase results in the greater stiffness that permits the notochord to elongate and straighten without being buckled by the surrounding tissues.

Key words: notochord, biomechanics, fiber density, osmotic activity, flexural stiffness, *Xenopus*, elongation.

Introduction

Morphogenesis results from the coordinated effects of mechanical forces exerted and resisted within the embryo. Plausible hypotheses about how these forces function in the embryonic development of animals have been made for the past hundred years (e.g. His, 1874; Rhumbler, 1902; Waddington, 1939; Lewis, 1947; Holtfreter, 1943, 1944; Gustafson and Wolpert, 1967; Phillips, 1984; Mittenthal and Jacobson, 1990) and, more recently, mathematical models of mechanical processes in morphogenesis have been proposed (e.g. Odell *et al.* 1981; Mittenthal and Mazo, 1983; Oster *et al.* 1983; White and Borisy, 1983; Oster and Odell, 1984; Belintsev *et al.* 1987). However, most of these ideas have not been tested experimentally, and a few that have were found to be in need of modification (e.g. Hardin and Cheng, 1986; Hardin and Keller, 1988). Although various techniques have been used to measure mechanical properties of individual cells (e.g. those reviewed by Bereiter-Hahn, 1987 and by Hiramoto, 1987; Harris *et al.* 1980; Nemoto *et al.* 1980; Tidball and Daniel, 1986; Sato *et al.* 1983), only a few studies have attempted to quantify the mechanical behavior of embryonic tissues (e.g. Waddington, 1939; 1942; Nogawa and Nakamishi, 1987) or of eggs (e.g. Rappaport, 1966; Hiramoto, 1976; Schroeder, 1981). We present here an empirical study of an important mechanical process during amphibian embryonic development: the elongation, straightening and stiffening of the notochord during the neurula and early tailbud stages.

Conflicting evidence on the role of the notochord in early development

The notochord (Fig. 1) appears to play a major role in the early morphogenesis of vertebrates, with evidence for this role being particularly strong in the amphibians. It is the first of the dorsal, axial tissues to differentiate in the amphibian. The notochord is initially distinguished from the prospective somitic mesoderm on either side by the unique shape and packing pattern of its cells, and by a distinct boundary that appears in the late midgastrula stage in *Xenopus laevis* (Youn *et al.* 1980; Keller, 1984; Keller *et al.* 1989). The dorsal axial mesoderm, of which the notochord is a large part, undergoes the morphogenetic movements of convergence (narrowing) and extension (lengthening) (Vogt, 1929; Schechtman, 1942; Keller, 1976; Wilson *et al.* 1989) which appear to function in closing the blastopore during gastrulation (Keller, 1985; Keller *et al.* 1985) and

in elongation of the neural plate during neurulation (Jacobson and Gordon, 1976; Jacobson, 1981; Keller and Danilchik, 1988). The dorsal mesoderm, including the prospective notochord, induces the formation of neural structures from the overlying ectoderm (Spemann, 1938). It has also been suggested that the notochord may function in elongation and straightening of the embryo during the post-neurula tailbud stages (e.g. Kitchen, 1949; Mookerjee, 1953). Moreover, the notochord is thought to function as a structural support (Bruns and Gross, 1970), and it may function in elastic energy storage during tadpole locomotion (Wassersug, 1989).

Despite the important mechanical roles attributed to the notochord, there is little direct evidence and some conflicting interpretations as to how it actually functions in early morphogenesis. The results of several studies are consistent with the notion that the notochord is involved in elongating the embryo. For example, experiments of Kitchen (1938, 1949), Horstadius (1944), Nieuwkoop (1946), and Mookerjee (1953) showed that the amphibian embryonic body failed to elongate in any region where the notochord had been removed. Similarly, tissues in the neural plate of the chick did not elongate after extirpation of the notochord (Jacobson, 1981), and tails of ascidian tadpoles from which the notochord had been removed surgically were greatly reduced in length (Reverberi *et al.* 1960). In addition, suppression of notochord development by lithium chloride treatment of amphibian embryos resulted in shortened embryos at the larval stages (Lehman and Ris, 1938), but it is not clear that this shortening was solely due to the defect in the notochord since other tissues are also affected by the same treatment.

In contrast, the interpretations of other studies are not consistent with the idea that the notochord is responsible for the elongation of early embryos. For example, extirpation and transplantation experiments on the tissues giving rise to the notochord, somites and neural tube of the amphibian tail (Bijtel, 1958) suggested that the somites and neural tube play an active part in tailbud elongation. Although removal of the notochord resulted in shorter embryos in these studies, Bijtel (1958) suggested that the notochord serves merely as a passive support or 'splint'. Moreover, embryos in which the boundary between the notochord and the somitic mesoderm does not form (a condition produced by ultraviolet irradiation of the early embryo) do not show significantly less axial elongation of the dorsal tissues than do normal embryos, at least through the late neurula stage (Malacinski and Youn, 1981; 1982; Youn and Malacinski, 1981). It should be noted, however, that the embryo-shortening effect of notochordectomy originally noted by Kitchen (1949) was not apparent until test embryos reached stages older than those examined by Malacinski and Youn.

Biomechanics of the embryonic notochord

In order to understand the *physical mechanisms* that produce shape changes during morphogenesis, we must first work out the mechanics of the components of the embryo that may participate in generating or resisting the forces driving particular morphogenetic events. Therefore, the first step we have taken towards working out how late neurula and early tailbud amphibian embryos elongate and straighten has been to analyze the mechanical development of the notochord during those stages. The rationale behind the particular measurements and experiments we performed can best be understood by first reviewing some basic biomechanical considerations.

Mechanical loading of the notochord

If elongation or straightening of the notochord are involved in generating the forces that lengthen the embryo, then the notochord acts as a column bearing a compressive load along its axis (Koehl *et al.* 1990). A slender column loaded in compression may bend or may undergo local buckling (i.e. kinking) if the force it is bearing is sufficiently large (e.g. Roark and Young, 1975; Wainwright *et al.* 1976; Gordon, 1978; Gere and Timoshenko, 1984). Therefore, the biologically important mechanical properties of the notochord are its flexural stiffness (resistance to bending) and its resistance to kinking. If a developing notochord is not sufficiently stiff, then it will not be able to elongate the embryo, but rather will remain bent or will be thrown into folds as it lengthens. Furthermore, even if the notochord is simply a passive skeletal rod rather than a force-generating structure, its flexural stiffness and its resistance to kinking are still the mechanical parameters of importance because they determine its performance both when loaded as a column (compressive force along its axis) and as a beam (lateral bending force). What features of the notochord are likely to determine its mechanical behavior?

The notochord as a hydrostatic skeleton

The structure of the notochord suggests that the morphological changes it undergoes during the early tailbud stages of development may be produced by a hydrostatic mechanism. The developing notochord (Fig. 1A and B) becomes encircled by a sheath, while its cells become vacuolated and enlarge. The fibrous sheath is composed of collagen and glycosaminoglycans (GAGs) (Weber, 1961; Bruns and Gross, 1970; Kenney and Carlson, 1978; Hay, 1984). In *Xenopus laevis* embryos, vacuolization of notochord cells begins during stages 23–24 (Nieuwkoop and Faber, 1967). The vacuoles appear to contain secreted GAGs (see Waddington and Perry, 1962); the high affinity of GAGs for water (Grodzinsky, 1983) suggests that enlargement of the vacuoles may involve osmotic uptake of water. Although it has been implied that increases in cell volume as vacuoles enlarge may force the notochord to elongate (Mookerjee *et al.* 1953), there is no evidence for the mechanical consequences of such inflation.

The notochord, which appears to be composed of a tension-resisting sheath containing compression-resisting material (cells) under pressure, is similar in basic design to the hydrostatic skeleton of various organisms (e.g. worms, herbaceous plants) and to man-made

pressure vessels (e.g. pneumatic columns, water tanks). A number of analyses have been conducted of the mechanical behavior of such hydrostatic skeletons (e.g. Clark and Cowey, 1958; Seymore, 1970; Swanson, 1974; Wainwright *et al.* 1976; Koehl, 1977; Hettiaratchi and O'Callaghan, 1978; Green, 1980; Alexander, 1987; Cosgrove, 1987; Wainwright, 1988; Wadepuhl and Beyn, 1989) and pressure vessels (e.g. Otto, 1962; Faupel, 1964; Sherrer, 1967; Roark and Young, 1975). These analyses point out a number of properties of cylindrical hydrostats that must be kept in mind as we consider the mechanics of the notochord (Koehl *et al.* 1990). We will briefly summarize these properties without formulating them quantitatively:

[A] The more resistant the walls of a hydrostat are to being stretched, the higher the internal pressure that can be sustained.

[B] The higher the internal pressure of a hydrostatic cylinder, the greater its flexural stiffness, and hence the larger the force required to bend it a given amount, both when loaded as a column (i.e. pushed along its length) and as a beam (i.e. pushed from the side).

[C] The higher the internal pressure, the larger the load ($\mathbf{F}_L$) it takes to kink a hydrostatically-supported column or beam.

[D] A limp hydrostatic cylinder can be straightened by inflation (unless the sheath is reinforced assymetrically).

[E] For a given internal pressure, the tensile stress (force per cross-sectional area of material being stretched) in a cylindrical sheath is twice as big in the circumferential direction as in the longitudinal direction. Therefore, if the sheath is isotropic, the cylinder when inflated increases in girth at a greater rate than in length (or it develops a local increase in diameter, i.e. an aneurism).

[F] The walls of both man-made and biological hydrostats are often reinforced with nearly inextensible fibers. The orientation of such fibers determines the shape changes that the cylinder undergoes when inflated.

[G] The deformation of a hydrostat in response to external forces can also be affected by the orientation of the sheath fibers. For example, a lower force ($\mathbf{F}_L$) is required to kink a hydrostatic cylinder reinforced with longitudinal and circumferential fibers than to kink one reinforced with the same density of diagonal fibers.

Objectives

As a first step towards elucidating the mechanism of elongation and straightening of late neurula and early tailbud amphibian embryos, we have investigated the biomechanical ontogeny of the notochord during these stages. We have focused on stages 21–28 of *Xenopus laevis* embryos (Nieuwkoop and Faber, 1967); these stages encompass the period after the convergence–extension of the notochord has taken place (Keller *et al.* 1989) and during which the notochordal sheath forms and cell vacuolization takes place (Mookerjee *et al.* 1953; Nieuwkoop and Faber, 1967). The objectives of this study were: (1) to quantify changes in the morphology of the notochord that correlate in time with the lengthening and straightening of the whole embryo; (2) to measure ontogenetic changes in the flexural stiffness of the embryonic notochord; (3) to determine the role of the notochordal sheath in constraining the shape and size changes the notochord undergoes; (4) to assess the role of osmotic swelling in lengthening, straightening, and stiffening the embryonic notochord.

Materials and methods

Collection and maintenance of embryos

Female *Xenopus* were injected with 750 units of human chorionic gonadotropin (Sigma) to induce ovulation. Twelve to fifteen hours later, eggs were squeezed out of the female into a Petri dish and fertilized with sperm obtained from the testis of a freshly killed male. Developing embryos were kept in large bowls of 25–33% modified Niu–Twitty solution (MNT, which is similar to Holtfreter's (1943) standard solution) at 23° C. Jelly coats were removed with 2.5% L-cysteine–HCl (Sigma) at pH 7.8. Embryos were staged according to Nieuwkoop and Faber (1967).

Morphometrics

Live embryos were cut along the midsagittal plane in room temperature 100% MNT and notochord diameter (Fig. 1) was measured immediately to the nearest 1.8 μm with an ocular micrometer fitted to a stereomicroscope. The embryo, including its notochord, was then drawn with a *camera lucida*. The notochord did not perceptibly change shape during this procedure. The length and diameter of the notochord, and the major and minor axes of the ellipses described by the dorsal edge of the embryo and of the notochord (Fig. 1C) were measured to the nearest 1.0 μm from the drawing using a Numonics digitizer interfaced with an Apple II computer. For each such ellipse, a 'straightness index' (**S.I.**) was calculated as the ratio of the major axis to the minor axis (Fig. 1C). Thus the **S.I.** increases in value as the notochord or embryo straightens.

Collagenase digestion of the notochord sheath

The dorsal tissues, including the notochord, somites and neural tube, were excised together (as described by Wilson *et al.* 1989) from some embryos, and the notochords were dissected from the somites and neural tubes of other embryos. These operations were done in baths of 1 mg ml^{-1} collagenase (Type I, Worthington Biochemical) plus 1 mg ml^{-1} trypsin (Type III, Sigma Chemical Co.) in MNT (1.2×10^{-1} osmol kg^{-1}, measured in a Wescor 5100B vapor pressure osmometer) at room temperature. The same enzyme lots were used for all the studies described here. In some cases the osmolality of the solution was increased by the addition of 0.5 M or 1.0 M sorbitol (Sigma) (osmolalities measured for these two solutions were 5.9×10^{-1} osmol kg^{-1} and 1.1 osmol kg^{-1}, respectively). The behavior of the tissues or isolated notochords in these various baths was recorded by a Panasonic NV-8050 time-lapse video recorder and camera on a Nikon compound microscope. Still photographs of the notochords were also taken on 35 mm Kodak Tri-X film, using a Zeiss stereomicroscope and automatic camera. The length and diameters (at distances from the anterior end of the notochord of one fourth, one half, and three fourths the length of the notochord) of each excised notochord were measured to the nearest 6 μm on enlarged, projected photo-

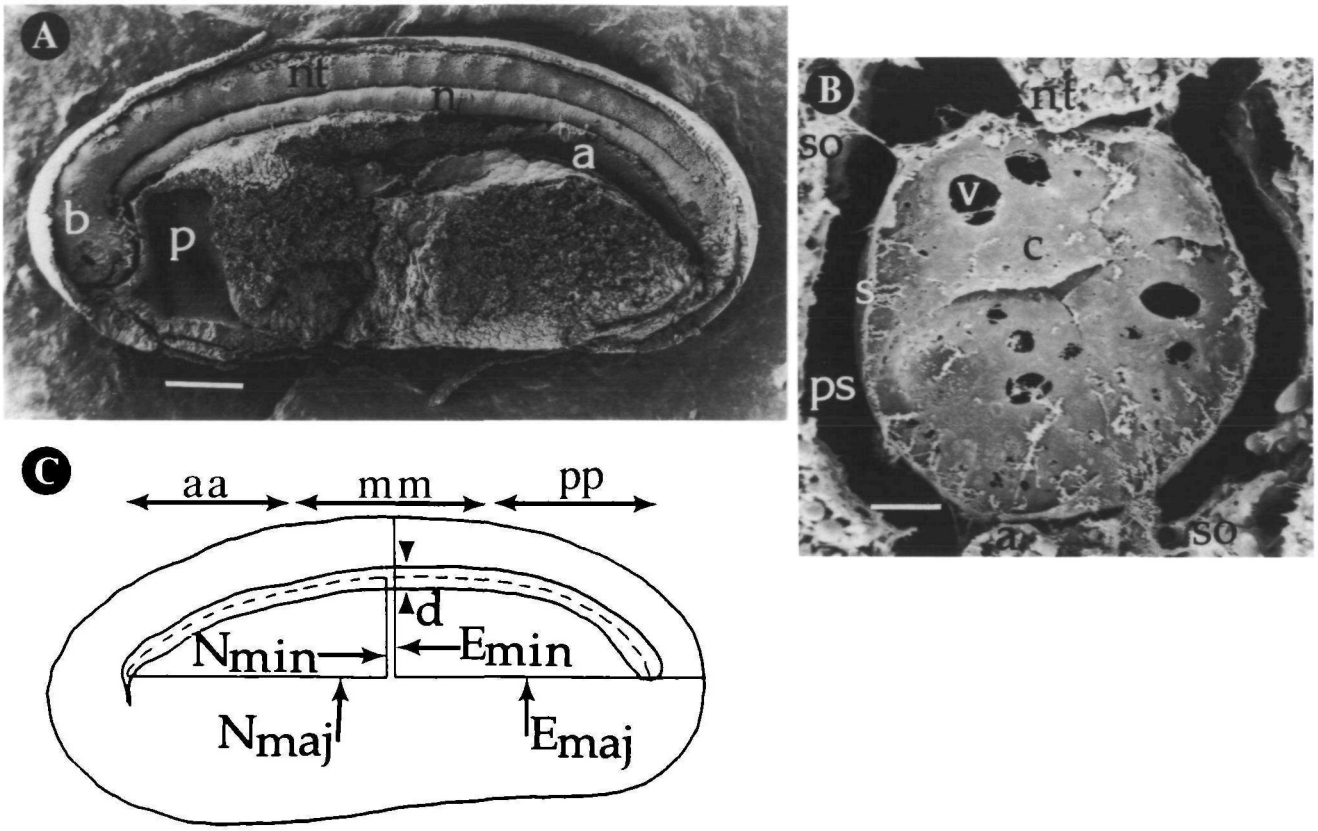

Fig. 1. Stage 24 *Xenopus laevis* embryo. (A) SEM of an embryo fractured sagittally just lateral to the notochord, showing the notochord (**n**), neural tube (**nt**), archenteron (**a**), pharynx (**p**), and the brain (**b**). Scale bar represents 200 μm. (B) SEM of the dorsal region of an embryo fractured transversely to show a cross-sectional view of the notochord, composed of a sheath (**s**) surrounding cells (**c**) containing vacuoles (**v**). Closely attached to the notochord are the overlying neural tube (**nt**) and underlying archenteron roof (**a**). Also shown are the perinotochordal space (**ps**) and the somites (**so**). Scale bar represents 10 μm. (C) Diagram of a sagittal view of an embryo illustrating the morphometric parameters used in this study: **d**=notochord diameter (between arrowheads); dashed line=notochord length; $\mathbf{N_{min}}$=half of the length of the minor axis of an ellipse described by the dorsal surface of the notochord; $\mathbf{N_{maj}}$=half of the length of the major axis of an ellipse described by the dorsal surface of the notochord ($2\times\mathbf{N_{maj}}$=distance from anterior to posterior end of curved notochord); $\mathbf{E_{min}}$=half of minor axis of ellipse described by dorsal surface of embryo; $\mathbf{E_{maj}}$=half the major axis of ellipse described by dorsal surface of embryo ($2\times\mathbf{E_{maj}}$=length of embryo). The anterior (**aa**), mid (**mm**), and posterior (**pp**) regions of the embryo are indicated by arrows above the diagram.

graphs taken after 15 and 30 min of emersion in a particular bath.

Scanning electron microscopy

After digestion in one of the solutions described above, the excised notochords and the excised tissue preparations were washed briefly in the same solution minus the enzymes, and fixed for 10 min in 2 %–2.5 % glutaraldehyde in 0.1 M sodium cacodylate buffer (pH 7.4). Other intact embryos were fixed with 2.5 % glutaraldehyde in 0.1 M sodium cacodylate buffer for more than 24 h and stored in the buffer until dissected. These specimens were cut along a sagittal plane, just lateral to the midline, to expose the lateral face of the notochord (Fig. 1A). All specimens were then dehydrated through an ethanol series, dried in a Polaron critical point dryer, mounted on stubs, and coated with about 3.0 nm of gold–palladium in a Polaron sputter coater. Scanning electron micrographs (SEMs) were taken with an ISI DS-130 scanning electron microscope using Polaroid 55 positive–negative film or Ilford sheet film.

Measurement of fiber angle

SEMs were taken of lateral surfaces of notochords from five embryos at each of the following four stages: 21, 23, 25, and 28. For each notochord, an SEM was taken within the anterior third, the middle third, and the posterior third (Fig. 1C). Micrographs were taken at 15 kV with a magnification of 4.7×10^3 and aligned with the long axis of each micrograph oriented parallel to the edges of the notochord in that region. Twenty five fibers in each micrograph were chosen using an overlay of computer-generated, randomly positioned points. The angle of each fiber with respect to the long axis of the notochord ('fiber angle') was measured to the nearest degree using a Numonics digitizer interfaced with an Apple II computer. Although the notochord sheath is very thin at the stages we examined (Fig. 1B), our measurements only reveal the orientation of the fibers that can be seen in SEMs of the outer surface of the sheath.

Measurement of fiber diameter and density

Fiber diameters on the SEMs mentioned above of the

notochord lateral surfaces were measured using a ruler, and fibers were divided into three size classes: small fibers were less than 0.2 μm in diameter, medium fibers were between 0.2 and 0.4 μm, and large were over 0.4 μm. Fiber density was estimated by drawing a line across the middle of each SEM parallel to the long axis of the notochord; the length of the line represented 20 μm on the SEM. The number of fibers crossing this line was counted and the size class of each fiber noted.

Measurement of flexural stiffness

Flexural stiffness (**EI**) is a measure of the resistance to bending of a unit length of a column or beam (e.g. Wainwright *et al.* 1976; Gordon, 1978). For non-hydrostatically supported columns and beams, **E** is the elastic modulus of the material from which the beam is constructed, and **I** is the second moment of area of the cross-section of the beam (a measure of the distribution of material around the axis of bending). However, for a hydrostatically supported cylinder (such as a notochord) whose stiffness also depends on internal pressure, we simply treat **EI** as a single parameter representing the resistance of a section of the structure to bending.

Notochords were dissected out of live embryos in 100 % MNT at room temperature and their flexural stiffness measured within 15 to 30 min. Each notochord was transferred with a pipette to the bending apparatus (Fig. 2A). The apparatus was made of plexiglas and coated with dimethyldichlorosilane (Sigma) to prevent sticking. The tip of a calibrated fiberglass needle was then used to bend the notochord through the notch in the apparatus (Fig. 2B), and the lateral deflection of both the notochord and the needle (Fig. 2C) were measured to the nearest 1.1×10^{-4} m using an ocular micrometer mounted in a stereomicroscope. The notochord was subjected only to small deflections (i.e. lateral displacement of the notochord midpoint was less than 10 % of the width of the notch in the apparatus).

To calculate the flexural stiffness (**EI**) of the notochord, the notochord was considered as a simply-supported beam subjected to a point load at its center (Fig. 2D). The **EI** of a beam subjected to such three-point bending is given by:

$$\mathbf{EI} = \mathbf{FL}^3/48\delta \qquad (1)$$

where **F** is the force (calculated from the deflection of the glass needle, as described below), **L** is the length of the beam between the two supports, and δ is the lateral deflection of the beam (Gordon, 1978).

The force-measuring glass needle was calibrated by measuring its deflection when bearing known weights at its tip. Polystyrene microspheres (Polybeads, Polysciences) were hung from the tip of the fiberglass needle by spraying the needle with water, touching the needle tip to a pile of beads, and then allowing the needle to dry. The needle was oriented so that the direction of deflection under the weight of the beads was the same as that during subsequent experimental measurements. The deflection of the needle by the beads was

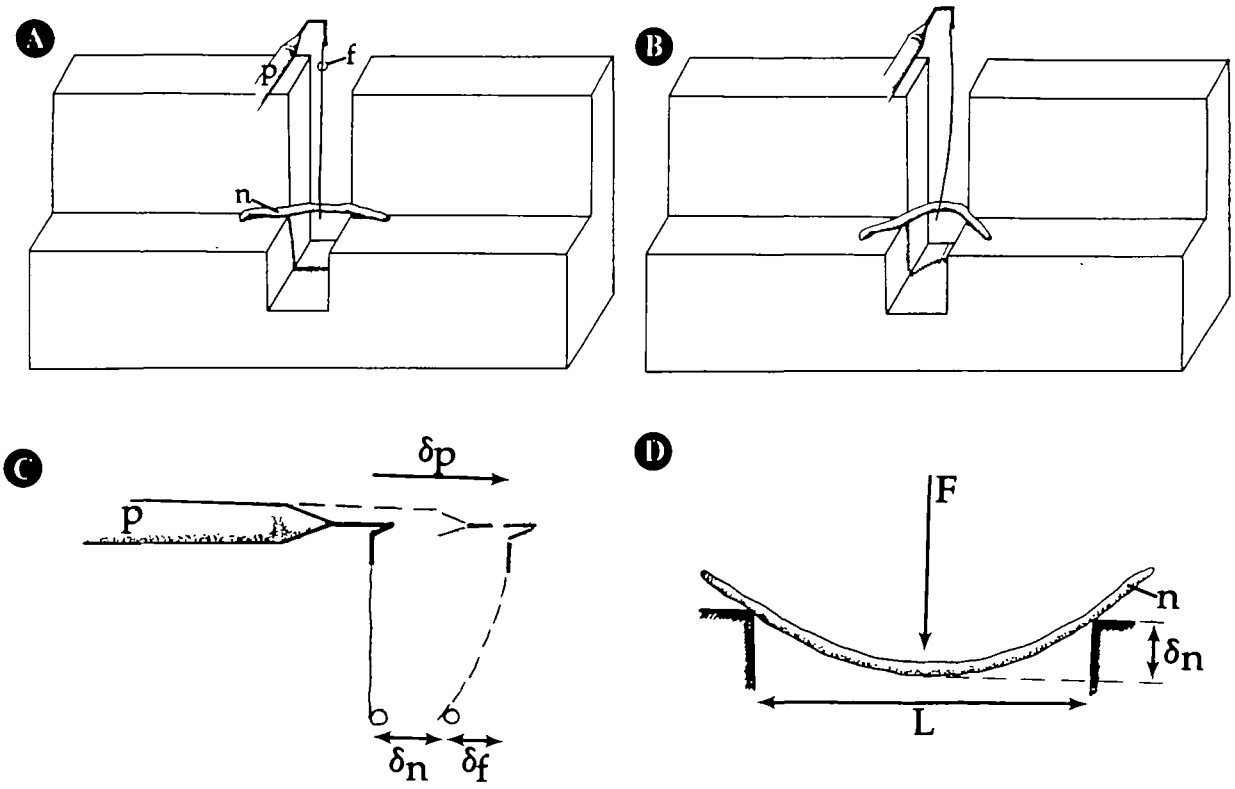

Fig. 2. Apparatus for determining flexural stiffness of excised notochords. (For clarity in these diagrams, deflections have been exaggerated and needle size reduced.) (A) A notochord (**n**) was placed across a slot in a block of plexiglass. A fiberglass needle (**f**) mounted on a pipette (**p**) moved by a micromanipulator was then brought in contact with the notochord at the midpoint of the gap, but no pressure was exerted. (B) The manipulator arm was then moved into the gap, bending the notochord. (C) The resulting deflection of the notochord (δ_n) was measured with an ocular micrometer. The deflection of the needle (δ_f) was determined by subtracting the deflection of the notochord (δ_n) from the displacement of the micromanipulator (δ_p). (D) Equation 1 (described in the text) was used to calculate the notochord flexural stiffness (**EI**) from the force applied (**F**, calculated from δ_f as described in the text), the length between the supports (**L**), and the deflection (δ_n) of the notochord.

measured to the nearest 1.1×10^{-4} m with an ocular micrometer in a horizontally mounted Zeiss stereomicroscope. Then the needle was drawn across a drop of water, dislodging the beads into the drop. The beads were then counted with a stereomicroscope and their total weight (w) was calculated:

$$w = NV\rho g \quad (2)$$

where N is the number of beads, ρ is the density of polystyrene (1.07×10^{-9} kg/m^3 (Polysciences)), g is the gravitational acceleration (9.81 m/s^2), and V is the volume of a single bead (each bead was assumed to be spherical, with a diameter of 8×10^{-6} m (Polysciences)). Larger deflections were generated by hanging a small length of hair from the tip of the needle. The downward force generated by the hair was calculated from the length used, measured to the nearest 1 μm with a Numonics digitizer interfaced with an Apple II computer, and the weight per unit length (N/m) of the same strand of hair (the mass of a hair 9.7×10^{-3} m long was measured to the nearest 1×10^{-6} g on a Cahn BE-74 electrobalance, model M-10). For each of the needles thus calibrated, a linear regression was calculated of force *vs.* deflection; each of these regressions had a slope significantly different from zero ($P\ll0.001$, $n=11$) and an r^2 value greater than 0.88.

Manipulation of osmotic environment

Notochords were dissected out of live embryos in 100 % MNT solution (1.2×10^{-1} osmol kg^{-1}) at room temperature. A *camera lucida* fitted to a Zeiss or Wild stereomicroscope was used to make drawings of the notochord in the embryo and of notochord after its excision from the embryo. The notochord was then transferred to a small dish of doubly distilled water, where it inflated osmotically to equilibration (i.e. ceased changing shape in 1 to 5 min). The inflated notochord was drawn again, and its **EI** was measured as described above. It was then transferred to a dish containing 100 % MNT solution and allowed to equilibrate; then it was drawn and its **EI** was measured again. Some inflation experiments were run in reverse order, i.e. the notochord was drawn and its **EI** was measured first in MNT and then in distilled water. Changes in notochord shape were also recorded with a Panasonic NV-8050 time-lapse video recorder.

Statistical analyses

The statistical tests we used (Statview and Systat statistical packages) are described in Zar (1974) and Sokal and Rohlf (1981). We used non-parametric tests in cases where data sets were small or of unknown distribution.

Results

Ontogenetic changes in morphology

(1) *Profile of the embryo and notochord*

Both the embryo and the notochord within it elongated and straightened between stages 21 and 28, as diagrammed in Fig. 3A. After stage 23 the straightness index (**S.I.**) of the embryo increased significantly (Fig. 3B). There was a concurrent straightening of the notochord, and we found a significant direct association between embryo **S.I.** and notochord **S.I.** (Fig. 3C).

(2) *Notochord dimensions*

Between stages 21 and 28, the period of notochord and embryonic straightening documented above, the notochord increased in volume about three-fold (Fig. 4A).

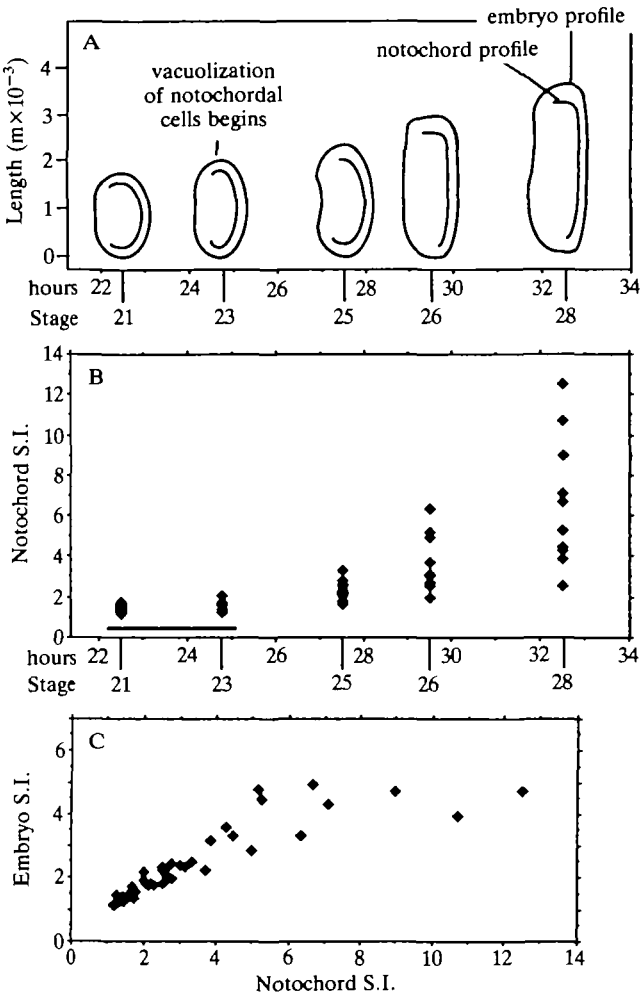

Fig. 3. Shape changes of the embryo and notochord. (A) *Camera lucida* diagrams of examples of profiles of embryos and of notochords at the stages indicated. Vacuolization has been reported to start at stage 23 (Niewkoop and Faber, 1967). (B) Straightness index (**S.I.**) of the notochord plotted as a function of time (hours at 25°C, and stage). Each point represents the **S.I.** of an individual notochord. The **S.I.** did not change significantly between stages 21 and 23 (as indicated by the bar below the data points), but did increase significantly between the subsequent stages (Kruskal–Wallis, Student–Newman–Keuls test, $H=40.29$, degrees of freedom (d.f.)=4, $P<0.001$). (Scatter of points in the high ranges of Fig. 3B and C, is due to the difficulty of defining the minor axis of the notochord in older animals in which the notochord was nearly straight at its posterior end.) (C) The straightness index (**S.I.**, defined in the text) of the embryo plotted against the **S.I.** of the notochord. There is a significant direct association between notochord **S.I.** and embryo **S.I.** (Kendall's tau test, $T=0.816$, $n=50$, $P<0.01$).

Notochord length began to increase significantly after stage 23, and diameter after stage 25 (Fig. 4B and C). The length-to-diameter ratio increased significantly only between stages 23 and 25 (Fig. 4D).

(3) *Notochord sheath*

The fibrous nature of the notochord sheath was obvious

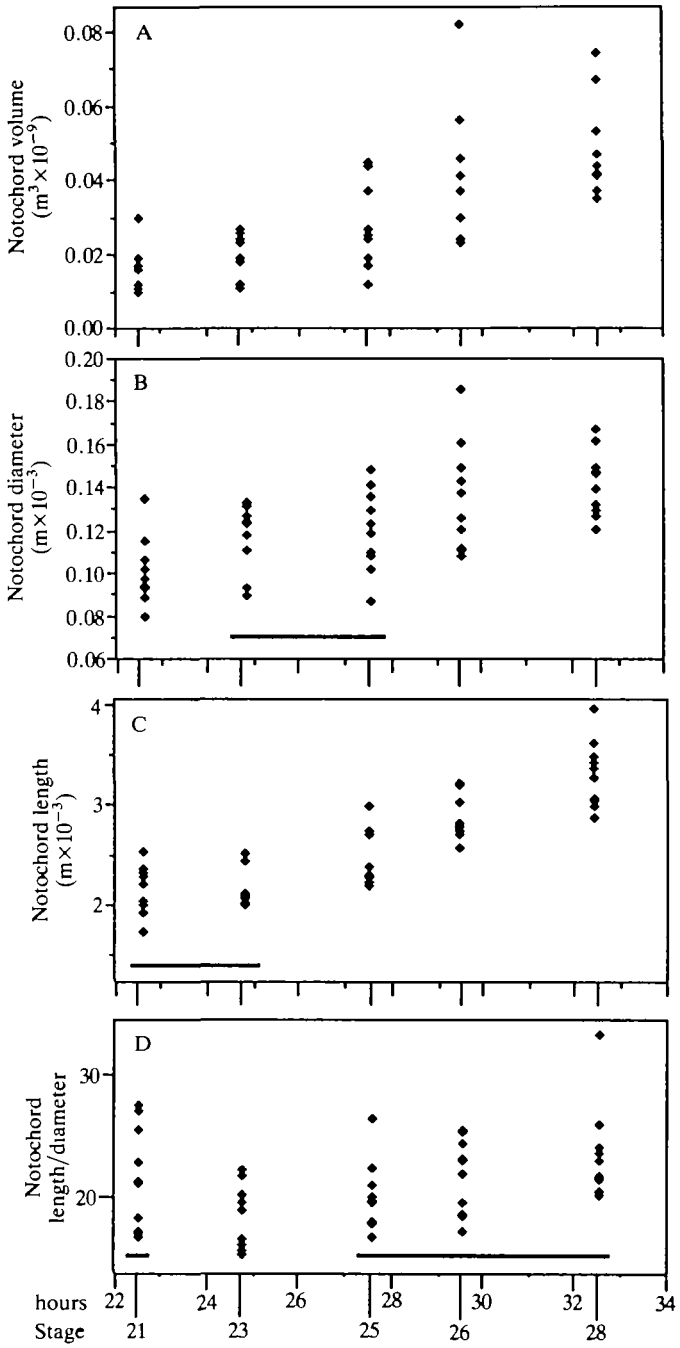

Fig. 4. Size changes of the notochord. (A) Notochord volume plotted as a function of time (hours at 25°C, and stage). Each point represents a different notochord. There was a significant increase in volume between each of the stages measured (Kruskal–Wallis, Student–Newman–Keuls test, $H=29.54$, d.f.=4, $P<0.0001$. (B) Notochord diameter plotted as a function of time. Each point represents a different notochord. There was a significant increase in diameter between all stages except between stages 23 and 25 (indicated by bar below data points) (Kruskal–Wallis, Student–Newman–Keuls test, $H=20.47$, d.f.=4, $P<0.025$). (C) Notochord length plotted as a function of time. Each point represents a different notochord. There was no significant increase in length between stage 21 and 23 (indicated by bar below data points), but there were significant increases in length between all subsequent stages measured (Kruskal–Wallis, Student–Newman–Keuls test, $H=37.65$, d.f.=4, $P<0.001$). (D) Notochord length-to-diameter ratio (**L/D**) plotted as a function of time. Each point represents a different notochord. **L/D** decreases significantly between stages 21 and 23, then increases significantly between 23 and 25, and thereafter does not change significantly (Kruskal–Wallis, Student–Newman–Keuls test, $H=11.99$, d.f.=4, $P<0.001$).

for all the stages (21–28) we investigated (e.g. Fig. 5A). Although we have not yet analyzed the chemical composition of the sheath, our enzyme digestions suggested that a major fibril component was collagen. We could remove the notochord sheath of early tailbud embryos (stages 21–23) with collagenase, although the collagenase did have some tryptic activity (assayed by Worthington at 0.4 i.u. mg^{-1} dry weight). Such removal of the sheath by collagenase, as determined by SEM, took longer and often was not complete in older embryos (R. Keller, unpublished data), suggesting that more collagen had been deposited, or that it was protected by other matrix material, or that other matrix material had become a significant part of the total. Digestion with trypsin alone (up to 1 mg ml^{-1} in calcium-free MNT) produced as much damage to the notochord cells and integrity of the notochord as it did to the sheath, and thus was not useful. However, we discovered by accident that 1 mg ml^{-1} trypsin in the collagenase solution accelerated the digestion of the sheaths on older stages while leaving the notochord cells intact (the trypsin may have had reduced activity because of the calcium in the collagenase solution). Therefore, we added 1 mg ml^{-1} trypsin to the collagenase solutions in all the sheath-removal experiments described below so that all stages of notochord could be compared in the sheathless state after 15 min digestion.

Fig. 5A illustrates the variety in diameter of notochordal sheath fibers. Although the density of slim fibers was significantly greater than that of wide ones, there was no significant relationship of fiber diameter or density with position (i.e. anterior, middle or posterior) on the notochord (Fig. 6A). There was a significant increase in the density of slim fibers at older stages (Fig. 6B).

Most of our SEMs of notochord sheaths revealed a wide range of fiber angles (angles between the fibers and the long axis of the notochord), as shown by the example in Fig. 5A and B. (There were a few cases of low angle variance, but there was no obvious pattern in the stage or notochord position where such cases occurred.) For the stages we examined, the distribution of fiber angles did not change significantly during development, nor did it differ significantly between anterior, middle and posterior regions of the notochord (Fig. 6C and D). In general, only a small proportion of the fibers were oriented at low angles with respect to the long axis of the notochord. The mean of all fiber angles (pooling all stages and positions) was 54°, which was significantly different from the 45° expected for randomly arranged fibers (99% confidence interval=52° to

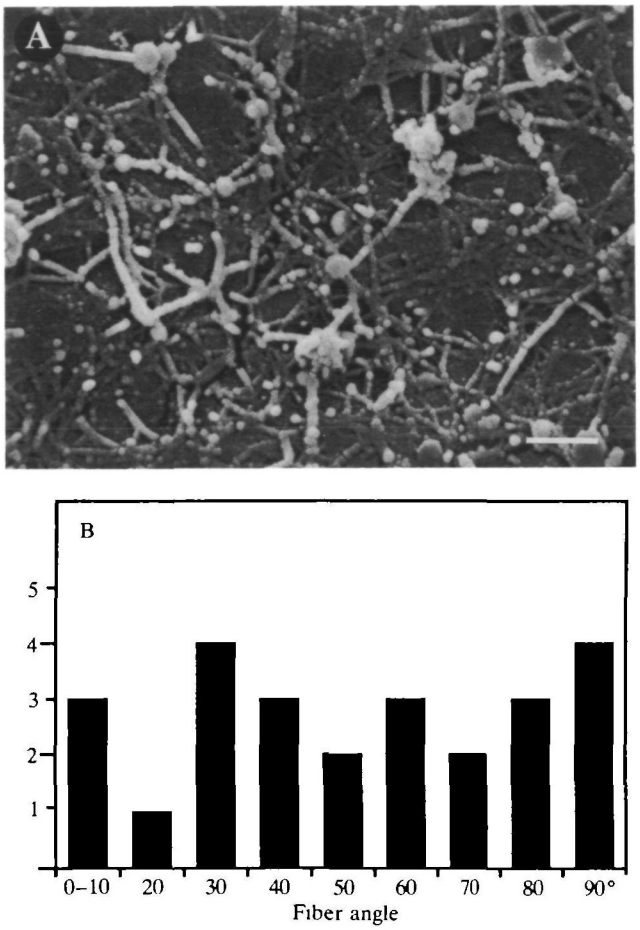

Fig. 5. Fibers in the notochord sheath. (A) SEM of the lateral surface of the sheath on the posterior region of the notochord of a stage 26 embryo. The bottom edge of the SEM is parallel to the long axis of the notochord. Scale bar=2 μm. (B) Histogram of the distribution of fiber angles (as described in the text) in the SEM shown in A.

57°, n=1500). Thus, the sheath was reinforced with diagonal fibers, a pattern that renders the notochord less likely to kink than would an arrangement of longitudinal and circumferential fibers.

Ontogenetic changes in flexural stiffness

The flexural stiffness (EI) of the notochord increased by an order of magnitude between stages 21 and 28, the significant increase occurring between stage 21 and 25 (Fig. 7). As mentioned above, stage 25 was also the first stage at which the notochord showed significantly increased length and straightness.

Role of the notochord sheath

(1) *Constraints of sheath fiber orientation on notochord shape changes*

When the fibers reinforcing the sheath of a hydrostatic cylinder are oriented at 54° to the long axis of the cylinder (as they were in *Xenopus* notochords at the stages we examined), their resistance to the circumferential and longitudinal tensile stresses caused by internal pressure are balanced (e.g. Faupel, 1964; Wainwright *et al.* 1976). Therefore, if the notochord behaves as a simple hydrostat whose shape changes upon inflation are determined by the sheath, then the notochord should inflate isometrically (i.e. its length-to-diameter ratio, **L/D**, should remain constant as it enlarges). Although the **L/D** of the notochord increased between stages 23 and 25, it did remain constant thereafter (Fig. 4D). Although these data suggest that, at least at stage 25 and later, the sheath limits the shape of the notochord, a more direct test of the role of the sheath can be made simply by observing the consequences of removing it.

(2) *Sheath limitation of notochord length*

The role of the notochord sheath in constraining the shape and size of the notochord at various stages of development was assessed by removing the sheath by digestion with collagenase and trypsin, as described above. Excised notochords (stages 21–26) whose sheaths were digested by a solution of these enzymes in 100% MNT underwent rapid lengthening. The sizes attained by such notochords after 30 min in the solution were generally no greater than those attained after 15 min (Fig. 8). In contrast, digested notochords at stage 18 (prior to sheath formation, Keller *et al.* 1989) did not elongate. Although the lengths of stage 21–26 notochords digested in MNT increased, their diameters did not. The latter observation is surprising, since a simple hydrostat should increase in girth at a greater rate than in width if the fibrous sheath is removed.

Role of internal pressure

(1) *Osmotic swelling of notochord cells*

To test whether the lengthening of sheathless notochords was due to osmotic uptake of water, we modified the osmotic strength of the MNT solutions in which the enzyme digestions were conducted by adding sorbitol, a metabolically inert compound which does not get into the cells and thus acts as an osmotic agent. Based on its composition, MNT (100%) is approximately of the same ionic strength as Holtfreter's standard solution, which is osmotically neutral with respect to most early amphibian cells (Holtfreter, 1943). Nonetheless, the lengthening of digested notochords could be prevented (or reversed) by the addition of sorbitol to the MNT bath before (or during) the digestion (e.g. Fig. 8A). These data indicate that notochord cells are more osmotically active than the other embryonic cells that do not swell in MNT.

Scanning electron microscopy of notochords after sheath digestion showed details of how the notochord cells changed shape in solutions of high and low osmolality. When notochords were digested in solutions in which they did not extend (e.g. Fig. 9E), the cells maintained the flattened 'stack-of-pizza-slices' appearance typical of cells in notochords with intact sheaths (Keller *et al.* 1989). The apices of such cells were elongated in the circumferential direction but were short in the direction parallel to the long axis of the notochord (Fig. 9G). In contrast, sheathless notochords that lengthened took on a helical configuration

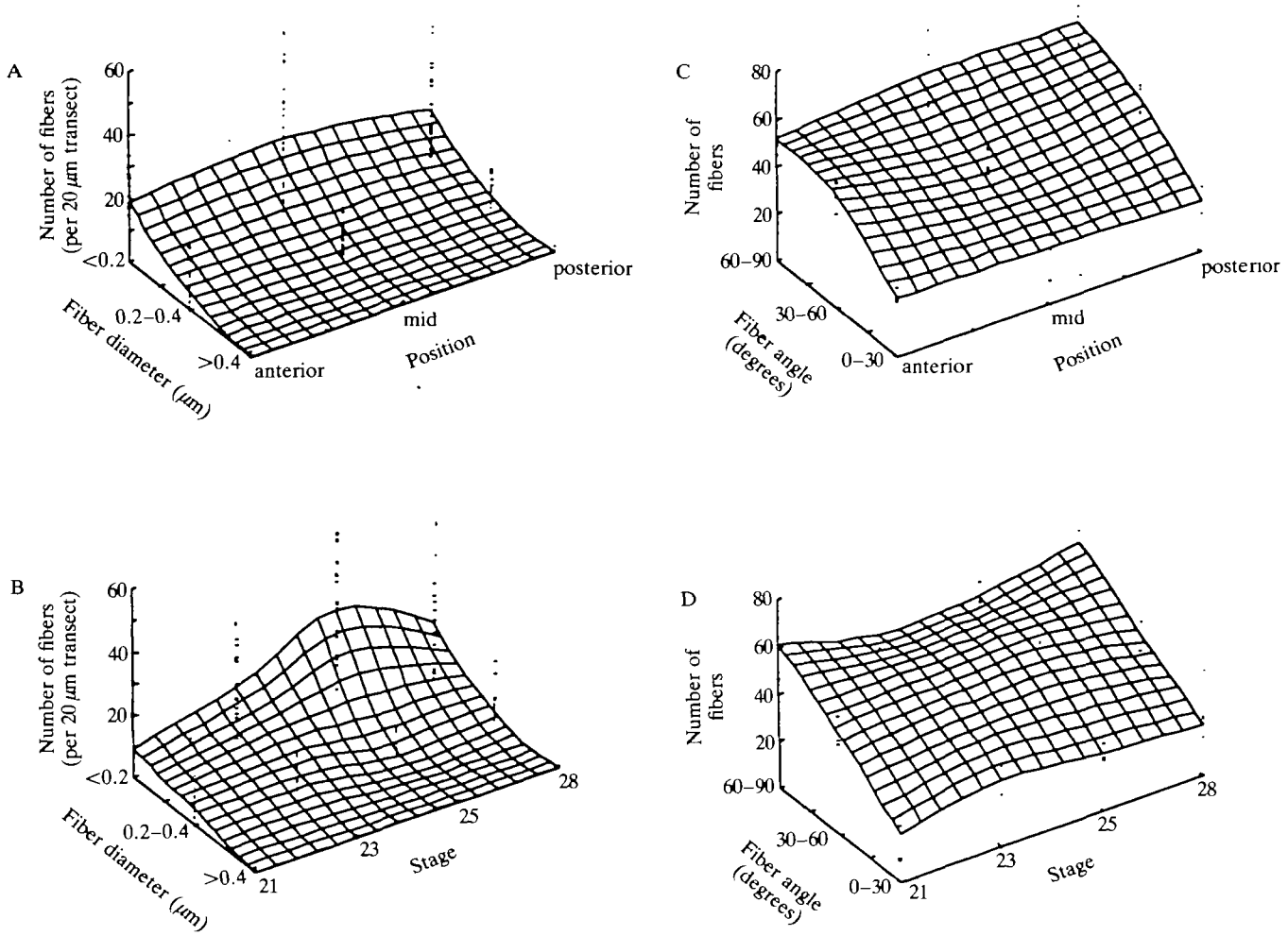

Fig. 6. Fiber density (number per 20 μm transect) in the notochord sheath, plotted as a function of fiber diameter and of (A) position on the notochord, and (B) stage of development. (Log-linear model, Pearson's Chi Square test showed the following interactions to be significant: density*diameter*stage, $P<0.009$; density*diameter, $P<0.001$.). Number of fibers at fiber angles of 0° to 30°, 31° to 60°, and 61° to 90°, plotted as a function of (C) position on the notochord, and (D) stage of development. Most fibers were at high angles, but there was no significant interaction between fiber angle and position or stage (log-linear model, Pearson's Chi Square test).

(Fig. 9F) and their cells became rounded (Fig. 9H). Higher magnifications of such cells revealed filiform and lamelliform protrusions forming junctions between cells (Fig. 9I). This connection of neighboring cells appeared to be responsible for the lack of increase in diameter by swelling sheathless notochords (Fig. 8B): a stack of flat cells connected to each other swelled into a configuration reminiscent of a string of pearls, longer but no wider than the original unswollen stack (diagrammed in Koehl *et al.* 1990).

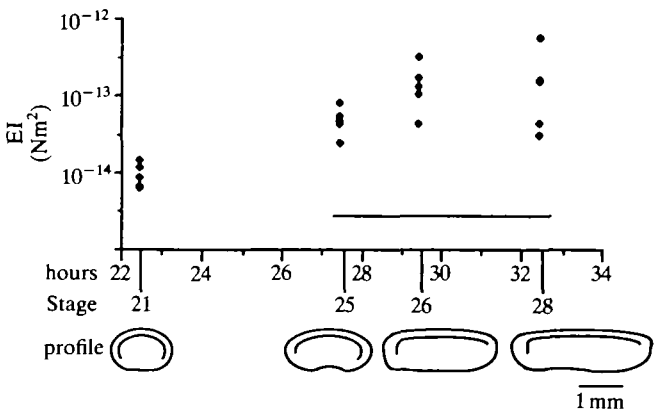

Fig. 7. Log of flexural stiffness (**EI**) plotted as a function of time (stage of development, and hours at 25°C). Each point represents a different notochord. Flexural stiffness increased significantly between stage 21 and 25 (Kruskal–Wallis, Student–Newman–Keuls test, $H=12.54$, d.f.=3, $P<0.025$), but not thereafter (as indicated by the bar below the data points).

(2) *Hydrostatic pressure in the notochord*

Our sheath-removal experiments showed that the tendency of the notochord cells to swell osmotically was prevented by the sheath. Therefore, at equilibrium, the osmotic pressure tending to drive water into the notochord is balanced by the hydrostatic pressure pushing

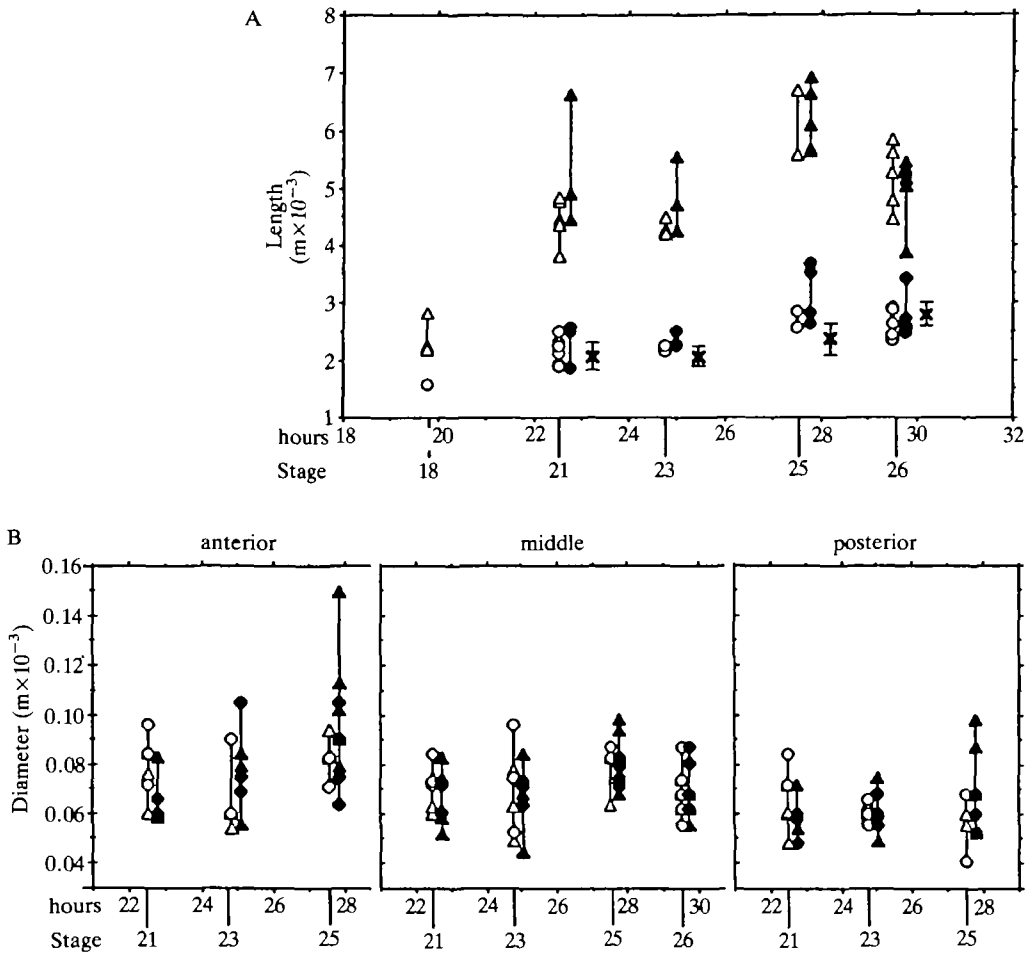

Fig. 8. (A) Lengths of isolated notochords whose sheaths have been digested in collagenase and trypsin in MNT (circles) or in MNT plus 1.0 M sorbitol (triangles). Notochord lengths after 15 min of digestion are shown by open symbols (connected by a line) and after 30 min by black symbols (connected by a line). The mean lengths of intact notochords in embryos (data shown in Fig. 4C) are indicated by 'x' for comparison (bars represent one standard deviation). Only at stage 23 was there a significant increase in length between 15 and 30 min of digestion. There was no significant difference between notochord length in media with and without sorbitol at stage 18, but lengths were significantly greater in media without sorbitol at all subsequent stages. (Mann–Whitney U test for all comparisons, $P<0.05$ for significance). (B) Diameters of the anterior, middle and posterior regions of notochords treated as described in A. Symbols are as defined in A. There was no significant difference between notochord diameters in media with *versus* without sorbitol at any of the stages examined (Mann–Whitney U).

Fig. 9. Micrographs of explants or isolated notochords digested by collagenase and trypsin in MNT or in MNT plus sorbitol. The anterior end of the embryos is to the right in A–D, the right side of the embryo is at the top in A–C, the dorsal surface of the embryo is facing the top in D, and the long axis of the notochord is parallel to the bottom of the page in E–H. The scale bar in A–F represents 100 μm, and in G–I represents 5 μm. (A) SEM of a ventral view of an explant of the top half of an early stage 20 embryo digested under a coverslip (see text) in MNT plus 0.5 M sorbitol, showing somites (**so**) and a straight notochord (**n**). (B) SEM of a ventral view of an explant of the top half of an early stage 20 embryo digested under a coverslip in MNT, showing the elongated, buckled notochord (**n**). (C) Light micrograph of a ventral view of an explant of the top half of a stage 21 embryo digested in MNT plus 1.0 M sorbitol in a dish unrestrained by a coverslip. The explant is flat and the notochord (**n**) is straight. (D) Light micrograph of a view from the right side of an explant of the dorsal half of a stage 21 embryo unrestrained by a coverslip and digested in MNT. The neural anlagen (**na**) has bent (with the dorsal surface on the inside of the bend), and the notochord (**n**) has elongated more than the surrounding tissues and has buckled. (E) SEM of a notochord excised from a stage 21 embryo and digested in MNT plus 1.0 M sorbitol. (F) SEM of a notochord excised from a stage 21 embryo and digested in MNT. (G) SEM of the apices of the cells (**c**) in the notochord shown in A. (H) SEM of the apices of the cells (**c**) in the notochord shown in B. (I) SEM showing filiform connections (**fc**) between cells (**c**) in the notochord shown in F.

out on the sheath. We estimated the hydrostatic pressure by using video recordings to determine whether notochords shrank or swelled when their sheaths were removed in solutions of different osmolalities. By subtracting the osmolality of a solution in which a notochord did not change dimensions from the osmolality of MNT (osmotically balanced with most embryonic amphibian cells), we calculated (as described by Nobel, 1970) the osmotic pressure tending to drive water into the notochord in the embryo. Such estimates indicated that the hydrostatic pressure in notochords in embryos at stages 18–21 ranged between 0.5×10^6 and

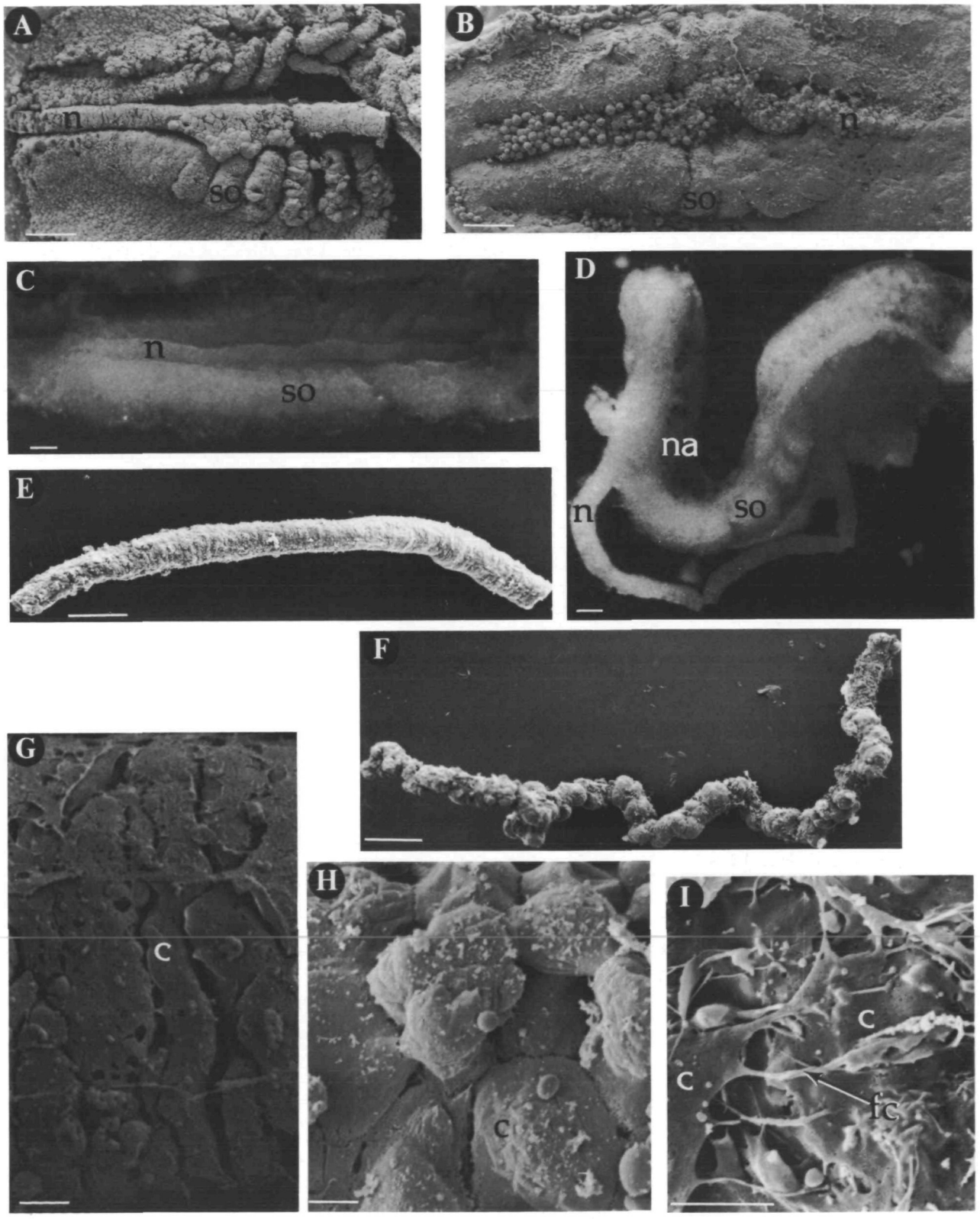

$1.2\times10^{6}\,N\,m^{-2}$, but increased thereafter (stages 23–26) to $2.4\times10^{6}\,N\,m^{-2}$. Hence, the internal pressure of the notochords rose two- to three-fold at the same period of development as their flexural stiffness increased by an order of magnitude, as their lengthening recommenced, and as their straightening began.

The pressures we estimated within the notochord sheath are relatively high. They are about an order of magnitude greater than those in *Xenopus* epidermal cells in culture (Strohmeier and Bereiter-Hahn, 1987), and are of the same order of magnitude as those in various plant cells (e.g. Nobel, 1970). To check whether our estimates of notochord internal pressure (**P**) were reasonable, we used them to predict the stresses in the notochord sheath. By estimating the thickness (**t**) of the sheath to be about 1.2 μm (measured on SEMs of notochord cross-sections) and using our measurements of notochord diameters (**D**), we calculated the tensile stresses in the sheath:

$$\sigma_H = (PD)/(2t) = 2\sigma_L \qquad (3)$$

where σ_H is the circumferential 'hoop' stress and σ_L is the longitudinal stress (Wainwright *et al.* 1976). Our estimates of stresses in the sheath were of the order of $10^{7}\,N\,m^{-2}$, which are within the range of stresses that have been reported for other collagenous connective tissues (e.g. Wainwright *et al.* 1976).

(3) *Notochord compared to neighboring axial tissues*

The osmotic elongation of notochords in 100 % MNT could reflect a behavior common to all axial tissues rather than a unique property of the notochord. When preparations of excised dorsal axial and paraxial tissue (in which endodermal epithelium was peeled off, leaving the notochord in its normal relation to the surrounding tissues) were placed in a bath of collagenase and trypsin in 100 % MNT, the notochord quickly elongated relative to the surrounding tissues (Fig. 9B). Elongating sheathless notochords did not appear to be stiff enough to stretch the surrounding tissues, but rather became buckled and folded as they lengthened. This elongation of sheathless notochords could be prevented by the addition of the appropriate concentration (see above) of sorbitol to the medium (Fig. 9A).

In the experiments described above, the deformation of an explant was somewhat limited because it was confined under a coverslip fragment supported on both ends by silicon high vacuum grease. However, when digested explants in MNT were unconstrained by the coverslip, the entire explant bent such that its outer surface was concave (Fig. 9D). This bending could be prevented by the addition of sorbitol to the medium (Fig. 9C), suggesting that the cells at the inner surfaces of the neural anlagen may have been swelling because they were hyperosmotic to the MNT (such bending also occurred when the notochord was separated from the explant). Nonetheless, the notochord lengthened more rapidly than the inner surface of the neural anlagen and stood away from it on its convex inner side. The bending of the unconstrained explant occurred at all stages, but the greater elongation of the notochord relative to the other tissues was characteristic only of explants made from stage 21 and older embryos, but not of younger embryos. This suggests that the osmotic properties of the notochord cells begin to diverge from those of the neural plate–neural tube cells in the late neurula stages (18–20).

(4) *Mechanical and morphological consequences of increasing notochord hydrostatic pressure*

Based on the data described above, we hypothesized that osmotic swelling of the notochordal cells (probably of the vacuoles therein) produces an increase in hydrostatic pressure within the fiber-wound notochordal sheath, with a consequent stiffening and straightening of the notochord. If this is true, then experimental osmotic inflation of curved young (e.g. stage 25) notochords should also produce a notochordal straightening and stiffening. An example of the shape changes that a stage 25 notochord underwent when placed alternatively in distilled water ($0\,osmol\,kg^{-1}$) and in 100 % MNT ($1.2\times10^{-1}\,osmol\,kg^{-1}$) is illustrated in Fig. 10; the notochord could be repeatedly straightened and unstraightened by manipulating its osmotic environment. As shown in Fig. 11, the osmotic inflation of excised stage 25 notochords mimicked the sorts of changes that occur during development: the notochord lengthened, widened, straightened and increased in flexural stiffness.

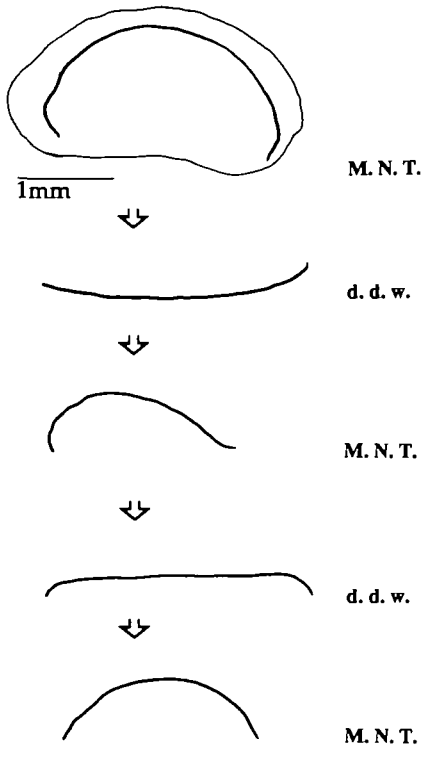

Fig. 10. *Camera lucida* drawings of a notochord in an embryo in 100 % MNT, and of that same notochord after being excised and placed in 100 % doubly distilled water (d.d.w.), then in 100 % MNT, then in 100 % d.d.w., and then in 100 % MNT.

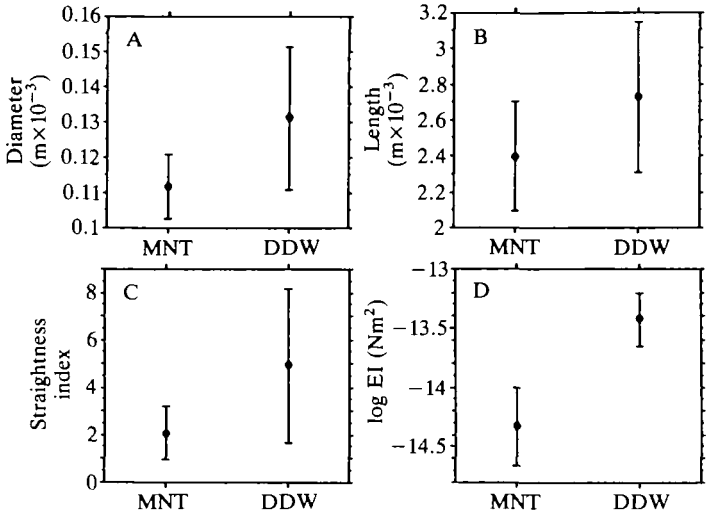

Fig. 11. Changes induced by osmotic inflation of notochords excised from stage 25 embryos. Bars represent one standard deviation about the mean (black circles) for five notochords placed first in 100% doubly distilled water (DDW) and then in 100% MNT for B and C. In A and D, 7 notochords were measured: five placed in DDW and then MNT, and two placed in MNT and then DDW. There was no significant difference for parameter values for notochords placed in MNT before DDW *versus* those placed in DDW before MNT (Wilcoxon Signed Rank test, $P<0.05$). (A) Diameters of notochords in DDW were significantly greater than they were in MNT (Wilcoxon Signed Rank test, $P<0.05$). (B) Lengths of notochords in DDW were significantly greater than they were in MNT (Wilcoxon Signed Rank test, $P<0.05$). (C) The straightness indices of notochords in DDW were more variable, but generally larger than they were in MNT (Wilcoxon Signed Rank, $P=0.076$). (D) The flexural stiffness (**EI**) of notochords in DDW were significantly greater than they were in MNT (Wilcoxon Signed Rank, $P<0.05$).

Discussion

Morphological and mechanical ontogeny of the notochord

(1) *Summary of changes in notochord properties*

The notochord of a *Xenopus* embryo undergoes a number of important changes between stages 21 and 25. During this interval in development, the notochord lengthens and straightens. Also at this time the density of fibers in the notochord sheath increases, and the sheath becomes more difficult to digest away. Concurrent with this reinforcement of the sheath, the osmotic activity of the notochord cells increases, the vacuoles within the cells enlarge, and the internal hydrostatic pressure of the notochord increases two- to three-fold. In addition, the flexural stiffness (**EI**) of the notochord increases by an order of magnitude between stages 21 and 25. Furthermore, the lengthening straightening and stiffening of the notochord that occur during the early tailbud stages of development can be mimicked by artificial inflation of excised notochords.

(2) *Biomechanical mechanism of notochord function*

Our measurements of the morphological and mechanical ontogeny of *Xenopus* notochords, coupled with the results of our sheath-removal experiments, lead us to propose the following mechanisms for the shape, size and stiffness changes that occur in the notochord during the early tailbud stages. The osmotic activity of the notochord cells increases, probably due to the secretion of GAGs into their vacuoles. Therefore, the flat cells in the notochord tend to swell osmotically. Because of the connections between adjacent cells in the notochord, such swelling tends only to lengthen the notochord. However, this lengthening is limited by the fibrous sheath surrounding the notochord. The resultant rise in internal pressure of the notochord increases its flexural stiffness. These changes in mechanical properties permit the notochord to elongate and straighten without being thrown into folds by the resistance of the surrounding tissues. Any forces resisting the elongation or straightening of the notochord would act along the length of the notochord, tending to bend or kink this skeletal rod. Our initial manipulations of excised notochords revealed that they were more easily bent than kinked. Therefore, we focused our attention on **EI** (flexural stiffness) rather than $\mathbf{F_L}$ (the critical force to produce local buckling) as the factor that would limit the ability of a lengthening notochord to straighten or to participate in forcing the elongation of the surrounding tissues of the embryo. The force required to hold a beam in a given bent configuration is proportional to $\mathbf{EI/L^3}$ (e.g. see equation 1), and the force necessary to initiate the elastic bending or bowing of a column ($\mathbf{F_E}$) is proportional to $\mathbf{EI/L^2}$ (e.g. Roark and Young, 1975; Gordon, 1978; Gere and Timoshenko, 1984). Hence, as notochord length (**L**) increases during development, substantially smaller forces can prevent it from straightening or can cause it to be thrown into bends unless its **EI** also increases. We found that the notochord **EI** does increase dramatically between stages 21 and 26, leading to a nine-fold increase in $\mathbf{F_E}$ (Koehl *et al.* 1990). Although we have not yet measured how notochord $\mathbf{F_L}$ changes during development, knowledge of the behavior of hydrostatic cylinders leads us to predict that the rise in internal pressure, coupled with an increase in sheath thickness, should lead to a rise in $\mathbf{F_L}$ with time. As mentioned above, the diagonal orientation of the fibers in the notochord sheath also render this skeletal rod resistant to kinking.

We see in the developing amphibian notochord an osmotic mechanism of force generation and shape-change production reminiscent of the hydrostatic mechanisms of morphogenesis in plants (e.g. Green, 1980; Cosgrove, 1987). Although the mechanical interactions between the notochord and the surrounding tissues remain to be measured, two types of observations are consistent with the idea that the notochord participates in generating the straightening and elongation of the early tail-bud amphibian embryo: (1) the notochord itself straightens and elongates forcefully, and (2) although the tissues surrounding the notochord appear

to elongate or bend during these stages without the notochord, (e.g. Bijtel, 1958; our Fig. 9D), they do not do so to as great an extent as they do when the notochord is present (e.g. Kitchen, 1938; 1949; Horstadius, 1944; Nieuwkoop, 1946; Mookerjee, 1953; Bijtel, 1958).

Significance of biomechanical analyses of axial structures

The axial mesoderm and the neural structures it induces constitute a powerful morphogenetic machine around which the rest of the embryo is organized from the gastrula and neurula stage onward (Jacobson, 1981; Keller, 1985; Keller and Danilchick, 1988), yet very little is known with certainty about the mechanics of either the neural or the mesodermal components. The evidence suggests a pressing need for more detailed analyses of the type presented here, on both passive and active mechanical properties of these tissues. For example, it has been proposed that axial stretching might function in neural tube closure (Jacobson, 1981), but there is no unambiguous biomechanical data to determine where such force is generated, if it is, and whether the mechanical properties of the tissues are consistent with such a mechanism. This comes at a time when the conventional wisdom about the biomechanics of tube closure has been called into question on numerous grounds (Schoenwolf and Smith, 1990). Moreover, there is evidence that mismatched growth rates of neural tubes and notochordal–endodermal components of the curly tail (ct) mutant in the mouse alters tail curvature and results in a high frequency of open neural tubes (Copp *et al.* 1988*a*,*b*). The defective curvature and closure can both be corrected by reducing the growth rate of both components to a uniformly low value with starvation (Copp *et al.* 1988*b*), implying that mechanical interaction of the extension rates in the two tissues are the primary cause of the failure of closure in this system, which is perhaps the best model system for human neural tube defects.

This work was supported by a University of California President's Undergraduate Fellowship and a National Science Foundation Graduate Opportunity Fellowship (to D. S. A.), NIH grants HD18979 and HD25594 (to R. E. K.), and a John Simon Guggenheim Memorial Foundation Fellowship, a Biomedical Research Support Grant, and NSF grant OCE8352459 (to M. A. R. K.). We are grateful to K. Baron, T. Daniel, J. Hardin, T. Hunter, R. Liu, E. Meyhofer, D. Pentcheff, C. Regen, J. Shih, W. Silk, and E. Thompson for advice or technical assistance.

References

ALEXANDER, R. McN. (1987). Bending of cylindrical animals with helical fibers in their skin or cuticle. *J. theor. Biol.* **124**, 97–110.

BELINTSEV, B. N., BELOUSSOV, L. V. AND ZARAISKY, A. G. (1987). Model of pattern formation in epithelial morphogenesis. *J. theor. Biol.* **129**, 369–394.

BEREITER-HAHN, J. (1987). Mechanical principles of architecture of eukaryotic cells. In *Cytomechanics* (ed. J. Bereiter-Hahn, O. R. Anderson, and W.-E. Reif), pp. 3–30. Berlin: Springer-Verlag.

BIJTEL, J. H. (1958). The mode of growth of the tail in urodele larvae. *J. Embryol. exp. Morph.* **6**, 466–478.

BRUNS, R. D. AND GROSS, J. (1970). Studies on the tadpole tail: 1. Structure and organization of the notochord and its covering layers in *Rana catesbiana*. *Am. J. Anat.* **128(2)**, 193–224.

CLARK, R. B. AND COWEY, J. B. (1958). Factors controlling the change of shape of certain nemertean and turbellarian worms. *J. exp. Biol.* **35**, 731–748.

COPP, A. J., BROOK, F. A. AND ROBERTS, H. J. (1988*a*). A cell-type specific abnormality of cell proliferation in mutant (curly tal) mouse embryos developing spinal neural tube defects. *Development* **104**, 285–295.

COPP, A. J., COROLLA, J. A. AND BROOK, F. A. (1988*b*). Prevention of spinal neural tube defects in the mouse embryo by growth retardation during neurulation. *Development* **104**, 297–303.

COSGROVE, D. J. (1987). Mechanical and hydraulic aspects of plant cell growth. In *Cytomechanics* (ed. J. Bereiter-Hahn, O. R. Anderson, and W.-E. Reif), pp. 215–229. Berlin: Springer-Verlag.

FAUPEL, J. H. (1964). *Engineering Design*. New York: John Wiley.

GERE, J. M. AND TIMOSHENKO, S. P. (1984). *Mechanics of Materials*, 2nd edn. Boston: P.W.S. Engineering.

GORDON, J. E. (1978). *Structures*. Middlesex, U.K.: Penguin Books Ltd.

GREEN, P. (1980). Organogenesis – a biophysical view. *Ann. Rev. Plant Physiol.* **31**, 51–82.

GRODZINSKY, A. (1983). Electromechanical and physiochemical properties of connective tissues. *CRC Critical Rev. Biomed. Engin.* **9**, 133–199.

GUSTAFSON, T. AND WOLPERT, L. (1967). Cellular movement and contact in sea urchin morphogenesis. *Biol. Rev.* **42**, 442–498.

HARDIN, J. D. AND CHENG, L. Y. (1986). The mechanisms and mechanics of archenteron elongation during sea urchin gastrulation. *Devl Biol.* **115**, 490–501.

HARDIN, J. D. AND KELLER, R. E. (1988). The behavior and function of the bottle cells during gastrulation of *Xenopus laevis*. *Development* **103**, 211–230.

HARRIS, A. K., WILD, P. AND STOPAK, D. (1980). Silicone rubber substrata: a new wrinkle in the study of cell locomotion. *Science* **208**, 178–179.

HAY, E. D. (1984). Collagen and embryonic development. In *The Role of Extracellular Matrix in Development* (ed. R. Trelstad), pp. 379–409. New York: Alan R. Liss.

HETTIARATCHI, D. R. P. AND O'CALLAGHAN, J. R. (1978). Structural mechanics of plant cells. *J. theor. Biol.* **74**, 235–257.

HIRAMOTO, Y. (1976). Mechanical properties of sea urchin eggs III. Viscoelasticity of the cell surface. *Develop. Growth Differ.* **18(4)**, 377–386.

HIRAMOTO, Y. (1987). Evaluation of cytomechanical properties. In *Cytomechanics* (ed. J. Bereiter-Hahn, O. R. Anderson, and W.-E. Reif), pp. 31–46. Berlin: Springer-Verlag.

HIS, W. (1874) *Unsere Korperform und das physiologische Problem ihrer Entstehung; Briefe an einen Befreundeten Naturforscher.* Leipzig: F.C.W. Vogel.

HOLTFRETER, J. (1943). A study of the mechanics of gastrulation. Part I. *J. exp. Zool.* **94**, 261–318.

HOLTFRETER, J. (1944). A study of the mechanics of gastrulation. Part II. *J. exp. Zool.* **95**, 171–212.

HORSTADIUS, S. (1944). Uber die Folge von Chordaextirpation an spaten Gastrulae und Neurulae von Ambystoma punctatum. *Acta Zool. Stolkh.* **25**, 75–88.

JACOBSON, A. G. (1981). Morphogenesis of the neural plate and tube. In *Morphogenesis and Pattern Formation* (eds. T. G. Connelly, L. Brinkley, and B. Carlson), pp. 223–263. New York: Raven Press.

JACOBSON, A. G. AND GORDON, R. (1976). Changes in the shape of the developing vertebrate nervous system analyzed experimentally, mathematically, and by computer simulation. *J. exp. Zool.* **197**, 191–246.

KELLER, R. E. (1976). Vital dye mapping of the gastrula and neurula of *Xenopus laevis*. I. Prospective areas and morphogenetic movements in the superficial layer. *Devl Biol.* **51**, 118–137.

KELLER, R. E. (1984). The cellular basis of gastrulation in *Xenopus laevis*: Active, postinvolution convergence and extension by mediolateral interdigitation. *Am. Zool.* **24**, 589–603.

KELLER, R. E. (1985). The cellular basis of amphibian gastrulation. In *Developmental biology: a comprehensive synthesis* (ed. L. Browder). New York: Plenum Press.

KELLER, R. E., COOPER, M., DANILCHIK, M., TIBBETTS, P. AND WILSON, P. (1989). Cell intercalation during notochord development in *Xenopus laevis*. *J. exp. Zool.* **251**, 134–154.

KELLER, R. E. AND DANILCHIK, M. (1988). Regional expression, pattern, and timing of convergence and extension during gastrulation of *Xenopus laevis*. *Development* **103**, 193–209.

KELLER, R. E., DANILCHIK, M., GIMLICH, R. AND SHIH, J. (1985). Convergent extension by cell intercalation during gastrulation of *Xenopus laevis*. In *Molecular Determinants of Animal Form, UCLA Symposia on Molecular and Cellular Biology, New Series* **31** (ed. G. M. Edelman), pp. 111–141. New York: Alan R. Liss.

KENNEY, M. C. AND CARLSON, E. (1978). Ultrastructural identification of collagen and glycosaminoglycans in notochordal extracellular matrix *in vivo* and *in vitro*. *Anat. Rec.* **190**, 827–850.

KITCHEN, I. C. (1938). The effects of extirpation of the notochord undertaken at the medullary plate stage in *Ambystoma mexicanum*. *Anat. Rec.* **72**, 34a.

KITCHEN, I. C. (1949). The effects of notochordectomy in *Ambystoma mexicanum*. *J. exp. Zool.* **112**, 393–415.

KOEHL, M. A. R. (1977). Mechanical diversity of the connective tissue of the body wall of sea anemones. *J. exp. Biol.* **69**, 107-125.

KOEHL, M. A. R., ADAMS, D. S. AND KELLER, R. E. (1990). Mechanical development of the notochord in *Xenopus* early tail-bud embryos. In *Biomechanics of Active Movement and Deformation of Cells* (ed. N. Akkas), pp. 471–485. Berlin: Springer-Verlag.

LEHMAN, F. E. AND RIS, H. (1938). Weitere Untersuchungen uber die Entwicklung der Achsenorgene bei partiell chordalosen Tritonlarven. *Rev. Suisse Zool.* **45**, 419–424.

LEWIS, W. H. (1947). Mechanics of invagination. *Anat. Record* **97**, 139–186.

MALACINSKI, G. M. AND YOUN, B. W. (1981). Neural plate morphogenesis and axial stretching in 'notochord defective' *Xenopus laevis* embryos. *Devl Biol.* **88**, 352–357.

MALACINSKI, G. M. AND YOUN, B. W. (1982). The structure of the anuran amphibian notochord and a re-evaluation of its presumed role in early embryogenesis. *Differentiation* **21**, 13–21.

MITTENTHAL, J. E. AND JACOBSON, A. G. (1990). The mechanics of morphogenesis in multicellular embryos. In *Biomechanics of Active Movement and Deformation of Cells* (ed. N. Akkas), pp. 295–401. Berlin: Springer-Verlag.

MITTENTHAL, J. AND MAZO, R. M. (1983). A model for shape generation by strain and cell-cell adhesion in the epithelium of an arthropod leg segment. *J. theor. Biol.* **100**, 443–483.

MOOKERJEE, S. (1953). An experimental study of the development of the notochordal sheath. *J. Embryol. exp. Morph.* **1**, 411–416.

MOOKERJEE, S., DEUCHAR, G. M. AND WADDINGTON, C. H. (1953). The morphogenesis of the notochord in amphibia. *J. Embryol. exp. Morph.* **1**, 399–409.

NEMOTO, S.-I., YONEDA, M. AND UEMURA, I. (1980). Marked decrease in the rigidity of starfish oocytes induced by 1-methyladenine. *Develop. Growth Differ.* **22**(3), 315–325.

NIEUWKOOP, P. D. (1946). Experimental investigations on the origin and determination of the germ cells, and on the development of the lateral plates and germ ridges in urodeles. *Arch. Neerl. Zool.* **8**, 1–205.

NIEUWKOOP, P. D. AND FABER, J. (1967). *Normal Table of* Xenopus *laevis (Daudin)*, 2nd ed. Amsterdam: North Holland Publishing Co.

NOBEL, P. S. (1970). *Introduction to Biophysical Plant Physiology*. San Francisco: W. H. Freeman.

NOGAWA, H. AND NAKAMISHI, Y. (1987). Mechanical aspects of the mesenchymal influence on epithelial branching morphogenesis of mouse salivary gland. *Development* **101**, 491–500.

ODELL, G. M., OSTER, G. F., ALBERCH, P. AND BURNSIDE, B. (1981). The mechanical basis of morphogenesis. *Devl Biol.* **85**, 446–462.

OSTER, G. F., MURRAY, J. D. AND HARRIS, A. K. (1983). mechanical aspects of mesenchymal morphogenesis. *J. Embryol. exp. Morph.* **78**, 83–125.

OSTER, G. F. AND ODELL, G. M. (1984). The mechanochemistry of cytogels. *Physica* **12D**, 333–350.

OTTO, F. (1962). *Tensile Structures*. Boston, M.I.T. Press.

PHILLIPS, H. M. (1984). Physical analysis of tissue mechanics in amphibian gastrulation. *Am. Zool.* **24**, 657–672.

RAPPAPORT, R. (1966). Experiments concerning the cleavage furrow in invertebrate eggs. *J. exp. Zool.* **161**, 1–8.

REVERBERI, G., ORTOLANI, G. AND FARINELLA-FERRUZZA, N. (1960). The causal formation of the brain in the ascidian larva. *Acta. Embryol. Morph. exp.* **3**, 296–336.

RHUMBLER, L. (1902). Zur Mechanik des Gastrulationsvorganges, insbesondere der Invagination. Eine entwicklungsmechanishe Studie. *Wilhelm Roux's Arch. EntwMech. Org.* **14**, 401–476.

ROARK, R. J. AND YOUNG, W. C. (1975). *Formulas for Stress and Strain*, 5th Edn. New York: McGraw Hill.

SATO, M., WONG, T. Z. AND ALLEN, R. D. (1983). Rheological properties of living cytoplasm: endoplasm of *Physarum polycephalum*. *J. Cell Biol.* **97**, 1089–1097.

SCHECTMAN, A. M. (1942). The mechanism of amphibian gastrulation. I. Gastrulation-promoting interactions between various regions of anuran egg (*Hyla regilla*). *Univ. Calif. Publ. Zool.* **51**, 1–39.

SCHOENWOLF, G. C. AND SMITH, J. L. (1990) Mechanisms of neurulation: Traditional viewpoint and recent advances. *Development* (in press).

SCHROEDER, T. E. (1981). The origin of cleaving forces in dividing eggs. A mechanism in two steps. *Expl Cell Res.* **134**, 231–240.

SEYMORE, M. K. (1970). Skeletons of *Lumbricus terrestris* L. and *Arenicola marine* L. *Nature* **228**, 383–385.

SHERRER, R. E. (1967). Filament-wound cylinders with axial-symmetric loads. *J. Compos. Mat.* **1**, 344–355.

SOKAL, R. R. AND ROHLF, F. J. (1981). *Biometry*, 2nd Edn. New York: W. H. Freeman.

SPEMANN, H. (1938). *Embryonic Development and Induction*. New York: Hafner.

STROHMEIER, R. AND BEREITER-HAHN, J. (1987). Hydrostatic pressure in epidermal cells is dependent on Ca-mediated contractions. *J. Cell Sci.* **88**, 631–640.

SWANSON, C. J. (1974). Applicaton of thin-shell theory to helically-wound fibrous cuticles. *J. theor. Biol.* **43**, 293–304.

TIDBALL, J. G. AND DANIEL, T. L. (1986). Elastic energy storage in rigored skeletal muscle cells under physiological loading conditions. *Am. J. Physiol.* **250**, 56–64.

VOGT, W. (1929). Chorda, Hypochorda und Darmentoderm bei anuren Amphibien. *Verh. Anat. Ges. Tubingen. Anat. Anz. Erg.* **67**, 153–163.

WADDINGTON, C. H. (1939). Order of magnitude of morphogenetic forces. *Nature* **3649**, 637.

WADDINGTON, C. H. (1942). Observations on the forces of morphogenesis in the amphibian embryo. *J. exp. Biol.* **19**, 284–293.

WADDINGTON, C. H. AND PERRY, M. M. (1962). The ultrastructure of the developing urodele notochord. *Proc. R. Soc. Lond. (B).* **156**, 459–482.

WADEPUHL, M. AND BEYN, W.-J. (1989). Computer simulation of the hydrostatic skeleton. The physical equivalent, mathematics, and application to worm-like forms. *J. theor. Biol.* **136**, 379–402.

WAINWRIGHT, S. A. (1988). *Axis and Circumference: The Cylindrical Shape of Plants and Animals*. Cambridge: Harvard University Press.

WAINWRIGHT, S. A., BIGGS, W. D., CURREY, J. D. AND GOSLINE, J. M. (1976). *Mechanical Design in Organisms*. Princeton: Princeton University Press.

WASSERSUG, R. J. (1989). Locomotion in amphibian larvae (or 'why aren't tadpoles built like fishes?') *Am. Zool.* **29**, 65–84.

WEBER, R. (1961). Similar pattern of fine structure in the basement lamella of the skin and the external sheath of the notochord in *Xenopus* larvae. *Experientia* **17**, 365.

WHITE, J. G. AND BORISY, G. G. (1983). On the mechanisms of cytokinesis in animal cells. *J. theor. Biol.* **101**, 289–316.

WILSON, P., OSTER, G. F. AND KELLER, R. E. (1989). Cell rearrangement and segmentation in *Xenopus*: Direct observation of cultured explants. *Development* **105**, 155–166.

YONEDA, M. AND DAN, K. (1972). Tension at the surface of the dividing sea urchin egg. *J. exp. Biol.* **57**, 575–587.

YOUN, B. W., KELLER, R. E. AND MALACINSKI, G. M. (1980). An atlas of notochord and somite morphogenesis in several anuran and urodelean amphibians. *J. Embryol. exp. Morph.* **59**, 223–247.

YOUN, B. W. AND MALACINSKI, G. M. (1981). Axial structure development in ultraviolet-irradiated (notochord-defective) amphibian embryos. *Devl Biol.* **83**, 339–352.

ZAR, J. H. (1974). *Biostatistical Analysis*. Englewood Cliffs, NJ: Prentice-Hall.

(*Accepted 30 May 1990*)